Community composition drives metabolic competition and *Staphylococcus aureus* colonization resistance in synthetic nasal communities

Marcelo Navarro Diaz[1,2,3], Kerrin Bertram[1,2,3], Laura Camus[1,2], Soyoung Ham[2,4], Lars Angenent[2,4,5,6,7], Jose Antonio Velazquez Gomez[2,4], Simon Heilbronner[1,2], Paolo Stincone[1,2], Johanna Rapp[1,2,3], Daniel Petras[1,2,8]*, Hannes Link[1,2,3]*

[1] Interfaculty Institute of Microbiology and Infection Medicine, University of Tübingen, 72076 Tübingen, Germany

[2] Cluster of Excellence "Controlling Microbes to Fight Infections", University of Tübingen, 72076 Tübingen, Germany

[3] M3 Research Center, University of Tübingen, Otfried-Müller-Str. 37, 72076 Tübingen, Germany

[4] Environmental Biotechnology Group, Department of Geosciences, University of Tübingen, Schnarrenbergstraße 94-96, 72076 Tübingen, Germany

[5] Max Planck Institute for Biology Tübingen, Max-Planck-Ring 5, 72076 Tübingen, Germany

[6] Department of Biological and Chemical Engineering, Aarhus University, Gustav Wieds Vej 10D, 8000 Aarhus C, Denmark

[7] The Novo Nordisk Foundation CO2 Research Center (CORC), Aarhus University, Gustav Wieds Vej 10C, 8000 Aarhus C, Denmark

[8] Department of Biochemistry, University of California, Riverside, 169 Aberdeen Dr., Riverside, CA 92507, USA

* Corresponding authors: dpetras@ucr.edu, hannes.link@uni-tuebingen.de

Abstract

The human nasal microbiome is a low-diversity ecosystem whose assembly principles and mechanisms of colonization resistance remain poorly understood. *Staphylococcus aureus* is a member of the nasal microbiome of some individuals with variable abundance. We hypothesized that nutritional competition, strain-level diversity, and nutrient availability shape community stability and the ability of commensal species to inhibit *S. aureus*. To test this, we constructed 50 defined synthetic communities composed of representative human nasal bacteria differing in strain and species composition and tracked their temporal dynamics, *S. aureus* growth, metabolic profiles, and nutritional interactions. The composition of synthetic communities with 5-10 species showed robust and reproducible dynamics and converged in one of three stable states. Synthetic communities dominated by a specific strain of *Corynebacterium propinquum* were highly stable and consistently excluded *S. aureus*. Growth curves and coculture assays showed that *C. propinquum* outcompetes *S. aureus* under poor nutritional conditions resembling the nasal environment, whereas *S. aureus* dominates in nutrient-rich conditions. Metabolomics analyses revealed that nutritional competition, including siderophores utilization and amino acid limitation, likely underlies this colonization resistance. These results establish a tractable synthetic community model for the human nasal microbiome and identify nutrient-dependent competition and microbial metabolite production as key drivers of community structure and pathogen exclusion.

Keywords

Nasal microbiome, *Staphylococcus aureus*, colonization resistance, Synthetic communities, metabolomics

55 **Introduction**

56 The human microbiome is important for human health and provides protection against
57 pathogens. This colonization resistance can occur through various mechanisms such
58 as nutritional competition or by use of inhibitory compounds [1]. Each anatomical site
59 contains distinct microbial communities composed of commensals, pathobionts, and
60 pathogens, which may be permanent residents or transient colonizers. Among these
61 sites, the nasal cavity is of particular interest because it is an entry point of airborne
62 pathogens such as *Staphylococcus aureus*, which is a major human pathobiont [2].
63 Approximately one-quarter of adults are persistently colonized with *S. aureus* in the
64 anterior nares, while others are intermittently colonized or remain uncolonized [3]. In
65 *S. aureus* carriers, the nasal cavity functions as a reservoir from which *S. aureus* can
66 disseminate to other body sites, occasionally leading to disease [4], which is especially
67 dangerous in immunocompromised and post-operation patients [5, 6].

68 Despite its clinical importance, the ecological and mechanistic factors that determine
69 the presence, absence, or abundance of *S. aureus* in the nasal microbiome are not
70 completely understood. Colonization resistance to *S. aureus* in the nose is a complex
71 process where the host's immunity has been shown to play a role [7], and several
72 species present in the nasal microbiome were shown to exhibit different types of
73 interactions with *S. aureus* [8]. Species reported to inhibit the growth of *S. aureus*
74 include *Staphylococcus lugdunensis* (which produces the antimicrobial lugdunin),
75 *Staphylococcus epidermidis* [8], and *Dolosigranulum pigrum* [9]. Other important
76 mechanisms of *S. aureus* exclusion, besides antimicrobial production, include nutrient
77 depletion [10, 11] and siderophore-mediated competition [12]. Such nutritional
78 competition is especially relevant in the context of the nasal environment, which has
79 been shown to be limited in carbon and energy sources, nutrients and iron, shaping

microbial interactions and colonization dynamics [10, 13]. However, disentangling these mechanisms *in vivo* and in the context of a whole microbial community is challenging, as the nasal cavity is a highly heterogeneous and host-specific environment that supports a comparatively small, but highly specialized, microbial community [14, 15].

By using synthetic communities (SynComs), the low-diversity nasal microbiome provides an ideal model to study fundamental ecological processes, such as community assembly, metabolic cross-feeding, and invasion dynamics. SynComs have been widely used to model other microbiome systems, such as the human gut microbiome [16, 17] and the rhizosphere of plants [18, 19]. These model systems have been instrumental in dissecting mechanisms of community assembly [18, 20], microbial function and metabolic interactions [21, 22], and responses to perturbations such as antibiotics or pathogen invasion [19, 23]. Previously, the PNC8 SynCom was developed as a model of the piglet nasal microbiome [24]. In contrast, to our knowledge there no SynComs for the human nasal microbiome, only pairwise pairwise cultures assembled from intrapatient strains [25]. Thus, an experimentally tractable SynCom system to study metabolic interactions and colonization resistance against *Staphylococcus aureus* in the human nasal ecosystem is currently lacking.

Seven community state types (CSTs) have been described for the human nasal microbiome based on species-level composition of *in vivo* datasets, suggesting recurring patterns of co-occurrence among dominant taxa [26]. However, these CSTs were defined on species-level resolution and do not account for strain-level variation, which may substantially influence ecological interactions and assembly dynamics. Whether nasal CSTs represent deterministic ecological attractors emerging from

105 intrinsic microbial interactions, or instead reflect host filtering and historical
106 contingency, remains unclear. To address this question, we adopted an unbiased
107 assembly strategy using prevalent nasal species combined randomly to test whether
108 stable community structures resembling in vivo CSTs would emerge from intrinsic
109 interaction dynamics and how such configurations influence resistance to *S. aureus*
110 invasion.

111 Here, we describe the development of a set of SynComs using a previously reported
112 culture collection of human nasal isolates [25]. We assembled 50 SynComs containing
113 random combinations of the most prevalent nasal bacterial species, each represented
114 by three distinct strains, and cultured them on agar plates containing a synthetic nasal
115 medium, previously developed to resemble the nutritional conditions of the nose [10].
116 After SynComs were established, we added *S. aureus* to test their colonization
117 resistance. We characterized their compositional and metabolic profiles using long-
118 read amplicon sequencing and untargeted and targeted metabolomics. Our approach
119 allowed us to identify key species, strain-level effects, and metabolite signatures that
120 are associated with abundance of *S. aureus* in the SynComs. These results provide a
121 tractable *in vitro* system to explore the ecological determinants of nasal community
122 assembly and pathogen exclusion.

123

124 **Methods**

125 *Bacterial pool selection*

126 To select species for SynCom construction, we first analyzed the Human Microbiome
127 Project (HMP) 16S rRNA amplicon sequencing data from the *nasal cavity* body site
128 [27]. Raw sequences were processed using QIIME 2 v2021.11 [28]. Quality filtering,
129 denoising, and chimera removal were performed with DADA2 [29], followed by
130 inference of amplicon sequence variants (ASVs). Taxonomic assignment was carried

131 out using BLAST [30] against the NCBI 16S rRNA RefSeq database [31]. The complete
132 ASVs table is provided in Supplementary Table S1.
133
134 Experiments were performed using bacterial isolates from the LaCa collection of nasal
135 bacterial isolates [25]. The LaCa collection comprises 228 isolates of bacteria (119
136 unique strains of 33 different species) from the nasal cavities of 11 healthy volunteers
137 [25]. We selected 10 of the most prevalent species based on our HMP analysis
138 (Supplementary Figure S1), with the limitation that they were available in the LaCa
139 collection and selecting 3 strains per species isolated from different volunteers to
140 ensure that isolates did not originate from the same population. For two species, for
141 which the LaCa collection did not have enough interpatient strains (*Corynebacterium*
142 *pseudodiphtheriticum* and *Corynebacterium tuberculostearicum*), we obtained 1 strain
143 from the German Collection of Microorganisms and Cell Cultures (DSMZ). These were
144 type strains *C. pseudodiphtheriticum* DSM44287 and *C. tuberculostearicum*
145 DSM44922.
146
147 *SynCom cultivation*
148 To avoid imposing predefined community structures, combinations were generated
149 randomly rather than replicating previously described CST compositions. Fifty
150 synthetic communities (SynComs) were assembled by randomly selecting both the
151 number (from 5 to 10) and identity of species, along with one randomly chosen strain
152 per species. This design enabled assessment of whether stable and recurrent
153 community configurations would emerge from intrinsic interaction dynamics across
154 strain backgrounds, thereby allowing evaluation of determinism versus contingency in
155 nasal community assembly. The experimental workflow is depicted in (Figure 1), and
156 species/strains used in each SynCom are listed in Supplementary Table S2.

157 Starter cultures were grown from glycerol stocks 24–72 h before experiments using
158 BHI, LB, or Columbia agar plates, depending on species (Supplementary Table S3).
159 Bacterial biomass was harvested from plates with sterile swabs, resuspended in PBS,
160 and adjusted to OD_{600} 1. Equal volumes (100 µL) of each strain suspension were
161 pooled to generate the SynCom inoculum. SynComs were plated in triplicate on
162 Synthetic Nasal Medium 3 (SNM3) agar plates, designed to mimic human nasal
163 secretions [10], and incubated for 72 h at 34°C. Inoculation of pooled cultures was
164 made on three SNM3 plates to obtain three technical replicates per SynCom. Biomass
165 was collected with sterile loops using a star pattern across the plate. This pattern
166 allowed us to collect enough biomass for DNA extraction while preserving enough
167 biomass for metabolomics analyses. Biomass was resuspended in 500 µL PBS and
168 used for reinoculation and DNA extraction. The rest of the biomass on the plate was
169 collected for metabolomics by transferring it into tubes containing 1mL of 80%
170 methanol and storing them at −80 °C until processing. Reinoculation consisted of
171 diluting the PBS suspension to OD_{600} 1 and plating 100 µL on fresh SNM3 plates. This
172 process was repeated for three sequential transfers. In the final transfer, SynComs
173 were challenged by inoculating *S. aureus* USA300 together with the SynCom
174 reinoculate at a 1000-fold lower OD. Staphylococcus aureus USA300 is a dominant
175 community-associated methicillin-resistant S. aureus (MRSA) clone that has emerged
176 as a leading cause of severe infections worldwide [32].
177
178 *Repetition experiment*

179 To evaluate reproducibility and analyze metabolites consumption profiles, five
180 SynComs were cultivated in a separate experiment using 12-well plates containing 2
181 mL of SNM3 agar per well. Culture initiation and sampling followed the same procedure
182 as in the main experiment, except that 20 µL of inoculum was used per well. Biomass
183 was collected from the wells for DNA extraction and reinoculation. For targeted
184 metabolomics, biomass was extracted by flooding from the wells with 2mL of 80%
185 methanol, incubated at −20 °C for 20 min, and processed as described above. Wells
186 without inoculum containing only SNM3 were analyzed as control. Additionally, *S.*
187 *aureus* USA300 and the three strains of *C. propinquum* were also grown as
188 monocultures in 12-well plates to analyze their metabolome. Three biological replicates
189 were used for each SynCom, control and monocultures.
190
191 *Co-cultures*
192 To test how the nutritional environment affected the interaction between *C. propinquum*
193 and *S. aureus*, we performed co-cultures between the 3 strains of *C. propinquum* used
194 in the SynCom experiments and *S. aureus* USA300. For these co-cultures we used
195 SNM3, SNM10 (which contained 3x or 10x more amino acids concentration of base
196 SNM), and the nutrient-rich medium BHI. We followed the same inoculation protocol of
197 the SynCom experiment after which we took biomass samples for DNA extraction and
198 sequencing. Three biological replicates were used for each of the co-cultures.
199
200 *Sequencing analyses*

201 DNA was extracted using the ZymoBIOMICS DNA Miniprep Kit (Zymo Research Corp.,
202 Irvine, CA, USA) following the manufacturer's protocol. Full-length rRNA operon
203 amplicons (~4,000 bp) were generated by PCR using primers 16S-27F-GGTGCTG-
204 ONT and 23S-2241R-GGTGCTG-ONT as described previously [33]. Nanopore
205 sequencing libraries were prepared with the Rapid Barcoding Kit (SQK-RBK114.96)
206 following the "Amplicon sequencing from DNA protocol" (available at
207 https://nanoporetech.com/document/rapid-sequencing-v14-amplicon-sequencing-
208 sqk-rbk114-24-or-sqk) and sequenced on MinION V14 flow cells (Oxford Nanopore
209 Technologies) using MinKNOW v25.05.14. Only reads with a quality score ≥10 were
210 retained and demultiplexed. Taxonomic classification was performed using Emu v3.4.5
211 [34] with a custom rRNA operon reference database generated from the strain
212 genomes via in silico PCR using EMBOSS-primersearch [35] as previously reported
213 [33].
214
215 Initial screening involved sequencing one replicate of the final time point (*i.e.*, after *S.*
216 *aureus* invasion) for each of the 50 SynComs. The complete table is provided in
217 Supplementary Table S4. Twenty representative SynComs were then selected for
218 sequencing of all time points and replicates. The complete table is provided in
219 Supplementary Table S5. Tables for the repetition experiment and coculture
220 experiments are available as Supplementary Table S6 and Supplementary Table S7
221 respectively. Raw fastq files from sequencing data are available in the NCBI SRA
222 database under the BioProject PRJNA1370791.
223
224 *Growth curves*

225 To analyze the differences in the growth of the species and their strains we performed
226 growth curves in SNM3. Biomass from reactivated strains was transferred using an
227 inoculation loop to BHI medium in a 5 ml culture tube and incubated overnight with
228 shaking at 220 rpm and at 37°C. Turbidity was assessed to ensure sufficient growth
229 before transferring 1.8 ml of medium to a sterile 2 ml Eppendorf tube. Cells were then
230 washed twice in SNM salts base (SNM without glucose or amino acids). The OD was
231 adjusted to 0.02 in SNM3 and cultures were transferred to a flat bottom 96-well plates.
232 Cultures were incubated at 37°C and shaken continuously at 269 cpm (6 mm). The OD
233 was measured every 10 min for 24 h using a BioTek SYNERGY H1 microplate reader
234 (Agilnet, Santa Clara, CA, USA). The complete tables for growth curve data is provided
235 in Supplementary Table S8 and Supplementary Table S9.
236
237 *Untargeted metabolomics*
238 For the samples of 20 selected SynComs, we sonicated the biomass suspended in
239 80% methanol for five cycles (60s on, 10 s off, 40% amplitude), centrifuged (10,000
240 rpm, 10 min), and supernatants were transferred to pre-weighed HPLC glass vials.
241 Methanol was evaporated under vacuum, and dried extracts were weighed and
242 resuspended to 5 mg/μL in 80% methanol.
243
244 Chromatographic separation was performed on a UHPLC system equipped with a C18
245 core-shell column (50 × 2.1 mm, 1.7 μm; Phenomenex). Solvent A was H_2O + 0.1%
246 formic acid, and solvent B was acetonitrile + 0.1% formic acid. The gradient increased
247 from 5% to 50% B over 8 min, then to 99% B by minute 10, followed by washing and
248 re-equilibration. Mass spectrometry was conducted on a Q-Exactive HF using heated
249 electrospray ionization in positive mode. MS1 scans were acquired at 60,000
250 resolution (120–1500 m/z). Data-dependent MS2 (Top 5) was performed with stepped

normalized collision energies of 25/35/45. Data were centroid-transformed with MSconvert and processed with mzmine v4.2.0 [36], and molecular networking was performed in GNPS 2 [37]. Chemical classification was inferred using CANOPUS [38] and SIRIUS [39]. The full feature table is available in Supplementary Table S10 and SIRIUS annotations are available in Supplementary Table S11. Raw data for untargeted metabolomics is available in MassIVE with accession number MSV000096776.

Biosynthetic gene cluster prediction

Biosynthetic gene clusters (BGCs) in *Corynebacterium propinquum* genomes were predicted using antiSMASH v8.0.2 with default parameters. Predicted clusters were classified according to antiSMASH annotations and similarity to reference clusters in the MIBiG database. Supplementary Table S12 contains the results for the Biosynthetic gene clusters (BGCs) predicted.

Targeted metabolomics of metabolites

Methanol extracts from the 12-well plates experiment were recovered, centrifuged, and stored at −80 °C until analysis. Metabolites were quantified by targeted LC-MS/MS on an Agilent TQ 6495 using a HILIC-Z column (2.1 × 150 mm, 2.7 µm; Agilent). Data was acquired using a subset of metabolites from the Agilent end-to-end targeted metabolomics workflow as described by Yannell et al. [40]. A table with peak intensities is found in Supplementary Table S13.

Statistical analyses

275 Amplicon data were analyzed in *R* v4.4.0 (using RStudio v2024.12.1). SynComs were
276 clustered based on relative abundances at the final time point using partitioning around
277 medoids (PAM) clustering implemented in the *cluster* R package [41]. The optimal
278 number of clusters was automatically determined using the Silhouette method [42],
279 selecting the number of clusters that maximized average silhouette width. Differential
280 metabolite abundance between SynCom clusters was analyzed using the *limma*
281 package [43]. Intensities were $\log_2$-transformed and quantile-normalized. Linear
282 models were fitted for each metabolite, and empirical Bayes moderation was applied
283 to obtain moderated t-statistics, $\log_2$ fold-changes, and Benjamini–Hochberg FDR-
284 adjusted p-values. Metabolites with FDR < 0.05 and $|\log_2 FC| > 1$ were considered
285 significantly associated with SynCom clusters. Multi-omics data integration and
286 visualization were performed in R using ggplot2 [44].
287

288 **Results**

289 *Nasal SynComs reflect the compositional diversity of the human nasal microbiome*

290 To develop SynComs that resemble the nasal microbiota, we used 5 to 10 bacterial
291 species, each represented by 3 different strains, each isolated from healthy individuals
292 (Figure 1). To identify most prevalent bacteria in the human nasal microbiome, we
293 performed a new analysis of the Human Microbiome Project data from the "nasal
294 cavities" body site (Supplementary Figure S1). We found that the nasal microbiome
295 showed high variability between studied individuals and that the composition is notably
296 uneven, with few species dominating most samples. Additionally, we found that,
297 although species alone did not completely explain *S. aureus* exclusion in the observed
298 samples, samples were grouped in at least broad 4 groups in terms of their
299 composition. Based on this, we selected a pool of 10 bacterial species (*Anaerococcus*
300 *octavius, Corynebacterium accolens, Corynebacterium propinquum, Corynebacterium*

301 *pseudodiphtheriticum, Corynebacterium tuberculostearicum, Cutibacterium acnes,*
302 *Cutibacterium avidum, Dolosigranulum pigrum, Staphylococcus epidermidis,*
303 *Staphylococcus lugdunensis*) that were prevalent in the human nasal microbiome with
304 the constraint that they were also present in the LaCa collection of nasal bacterial
305 isolates [25].
306
307 Next, we assembled 50 SynComs by pooling 5 to 10 randomly selected species and
308 one random strain per species and growing them in synthetic nasal medium (Figure
309 1). To evaluate the stability and assembly process of the SynComs, they were cultured
310 iteratively 4 times with reinoculations in fresh plates every 3 days to ensure sufficient
311 supply with nutrients. In the last reinoculation, we added *S. aureus* to test the
312 colonization resistance of the SynComs. We characterized the composition of the
313 communities at the final time point (72 h after *S. aureus* was added, Figure 1). Across
314 randomly assembled communities, we observed variable end-point composition, with
315 some SynComs converging toward stable multi-species composition while others
316 became dominated by a single species (Figure 2). The SynComs were grouped in
317 three clusters (compositional similarity with silhouette method) with different species
318 richness, evenness, dominant species and different resistance to *S. aureus*
319 colonization (Figure 2). Importantly, SynComs with similar inocula at the species-level
320 resulted in different end-point compositions, thus indicating a large influence of strain-
321 level variation. For instance, SynComs that contained all the 10 species
322 (Supplementary Table S2) with different strains that lead to different final compositions
323 and cluster belonging included SC1 (Cluster 1), SC29 (Cluster 2), SC5 (Cluster 3).
324
325 The end-point composition of the 50 SynComs clustered in three distinct groups.
326 Cluster 1 was dominated by *C. propinquum* (mean of 93.1%) and showed high

327 resistance to *S. aureus* (mean abundance of 4.6%, Figure 2). Just a few other species
328 occurred at low abundance in cluster 1 SynComs (*e.g.*, *Staphylococcus lugdunensis*
329 and *S. epidermidis*). Thus, the 20 SynComs of cluster 1 consisted primarily in co-
330 cultures of *C. propinquum* and *S. aureus*. The other two clusters showed higher
331 species diversity. Cluster 2 frequently included *S. lugdunensis*, *C.*
332 *pseudodiphtheriticum*, *C. avidum*, *D. pigrum*, *C. accolens*, and *C. tuberculostearicum*.
333 This cluster had the lowest colonization resistance, with a mean relative abundance of
334 *S. aureus* of 34.1%. Cluster 3 included similar species as cluster 2 but was dominated
335 by *S. epidermidis* and *S. lugdunensis*. Cluster 3 showed strong colonization resistance,
336 with a mean final relative abundance of *S. aureus* of 6.9%. Two bacterial species *A.*
337 *octavius* and *C. acnes* were not detected in any SynCom.
338
339 *Strain-level diversity influenced population dynamics and resistance to S. aureus*
340 *colonization*
341 Next, we selected 20 representative SynComs that captured the compositional
342 diversity of the full data set. We characterized their composition at all time points, which
343 included the 4 samples taken every 72 h when sampling for biomass to reinoculate the
344 SynComs in fresh SNM3 plates. For these SynComs, we sequenced all time points
345 and replicates. Figure 3 shows one replicate per SynCom and time point.
346 Supplementary Figure S2.A shows the Bray-Curtis distance between the replicates
347 which was below 0.2 for most of the SynComs, showing reproducibility of our
348 experimental setup.
349
350 Sequencing of the 20 SynComs revealed that both species and strain identity had a
351 substantial impact on SynCom assembly and composition. In addition to Figure 3,
352 Supplementary Figure S2.B shows the Bray-Curtis distance between the first three

353 timepoints and the final composition for all sequenced SynComs. In general, there
354 were two types of assembly patterns, one that stabilized quickly after timepoint 1 and
355 another that varied at the 4 time points. The first group (SynComs 7, 9, 11, 12, 14 and
356 22) with fast stabilization included SynComs that were dominated by *C. propinquum*
357 strains 16 and 265. These SynComs showed low dissimilarity values from the
358 beginning of the experiment compared to the final state. The other SynComs showed
359 less stable dynamics with a more fluctuating composition and higher dissimilarity
360 values in respect to the final state, which was dependent on the species and strains
361 inoculated.
362
363 Next, we observed that strain-level variation played an important role for assembly of
364 the different SynComs. For example, the presence of distinct strains of the same
365 species had a strong effect on the abundance of *S. aureus* at the final time point. The
366 strongest strain-level effect observed was the case of *C. propinquum* in cluster 1, in
367 which all except for one of the SynComs consisted of two *C. propinquum* strains (Nr.
368 16 and Nr. 265; Figure 2). In contrast, *C. propinquum* strain 70 was present only during
369 the initial time points and other species overgrew it by the end of the experiment (for
370 example SynComs 13, 23 and 50, Figure 3). Thus, *C. propinquum* strain 70 only
371 dominated in SynCom 6 (Figure 2). Similarly, *D. pigrum* strain 21 was the only strain
372 of this species that could persist through the entire cultivation period in the SynComs
373 where it was included, although its abundance was always below 5%. *D. pigrum*, *A.*
374 *octavius* and *C. acnes* are fastidious bacteria and neither of their strains showed
375 growth when we tried growing them as monocultures in SNM3 (Supplementary Figure
376 S3). Thus, in the case of *D. pigrum*, strain 21 was able to grow only when it was part
377 of these specific SynComs when growing in SNM3, suggesting that it obtains essential
378 nutrients or cofactors from other bacteria in these communities. Additionally, we

379 observed co-occurrence patterns at species level such between *C. accolens*, *C.*
380 *avidum*, *C. pseudodiphtheriticum*, and *D. pigrum*, independently of the strains used for
381 the first two species (for example in SynComs 19, 25, 27, 44 and 50).
382
383 We then performed co-cultures between each of the 3 strains of *C. propinquum* and *S.*
384 *aureus* USA300 to explore how the nutritional environment can affect the interaction
385 between these two species. *C. propinquum* strains 16 and 265 (but not strain 70) were
386 able to dominate over *S. aureus* under the nutritional conditions of SNM3
387 (Supplementary Figure S4). In BHI medium, in contrast, *S. aureus* dominated the
388 pairwise co-cultures against all three *C. propinquum* strains (Supplementary Figure
389 S4). Additionally, the *C. propinquum* strains 16 and 265 achieved higher optical
390 densities after 24 h growth in liquid medium than strain 70 (Supplementary Figure S3).
391
392 *Metabolome of SynComs differs between clusters and suggests nutritional competition*
393 To investigate the metabolism of the different SynComs, we performed untargeted
394 metabolomics on all time points and replicates of the 20 selected SynComs (Figure 4).
395 Metabolite extracts in methanol:water were collected from plates and analyzed by
396 untargeted LC–MS/MS enabling comprehensive detection of small-molecule features
397 without prior assumptions about metabolite identities.
398
399 We used Linear Models for Microarray Data (limma) to test whether the identified
400 SynCom clusters according to microbial composition (Figure 2 and Figure 4A) differed
401 in their metabolic profiles. Limma applies linear modeling and an empirical Bayes
402 method to detect features that differ significantly between predefined groups while
403 accounting for variance and multiple testing. This analysis showed that each cluster of
404 SynComs has a distinct metabolic signature (Figure 4B). Especially SynComs from

405 Cluster 1, which were dominated by *C. propinquum*, showed enrichment of specific
406 metabolites such as the siderophore deferoxamine E, indicating that this metabolite is
407 associated with high abundance of *C. propinquum* in these communities. In the
408 genomes of the three *C. propinquum* strains, seven biosynthetic gene clusters (BGCs)
409 were predicted using antiSMASH. In particular, one high-confidence NI-siderophore
410 cluster showed strong similarity to the dehydroxynocardamine biosynthetic pathway,
411 consistent with the detection of deferoxamine E in the untargeted metabolomics data.
412 Annotation with SIRIUS predicted that the other compounds associated with the
413 SynCom clusters are mainly amino acids, their derivatives, and peptides.
414
415
416 *Metabolites production and consumption profiles are SynCom-specific and influence*
417 *S. aureus colonization resistance*
418 To assess the role of amino acids and other metabolites on the nutritional competition
419 in community assembly and *S. aureus* colonization resistance, we analyzed a panel of
420 24 nutrients involved in primary metabolism of bacteria, including amino acids,
421 nucleosides, and vitamins for 5 selected SynComs (Figure 5 and Supplementary Table
422 S10). These 5 SynComs were representative from clusters 1 (SC7 and SC12) and
423 cluster 3 (SC27 and SC40) that showed high *S. aureus* colonization resistance and 1
424 SynCom from cluster 2 (with low *S. aureus* colonization resistance). Importantly, when
425 we cultured these 5 SynComs for this metabolomics experiment, their composition
426 matched the results from the main experiment, demonstrating the reproducibility of the
427 cultivation protocol and SynCom stability (Figure 5A). Additionally, we measured the
428 24 compounds in monocultures of *S. aureus* USA300 and the three *C. propinquum*
429 strains used in the SynCom experiments. Using 12-well agar plates, we quantified
430 concentration changes of the 24 nutrients relative to their starting concentrations in the

431 medium (measured in control wells without inoculum; Figure 5B and 5C). These data
432 showed that some nutrients are increasing relative to the medium, indicating that they
433 are produced by specific bacteria. For example, all 5 SynComs and the three *C.*
434 *propinquum* strains had high levels of riboflavin and tyrosine, which were hardly
435 measurable in the medium and in *S. aureus* cultures.
436
437 Other nutrients were depleted in *S. aureus* cultures relative to the medium, such as
438 alanine, glutamic acid, and glycine. SynComs 10 and 12, which were dominated by *C.*
439 *propinquum*, showed strong decreases of several nutrients (at least 4-fold change in
440 10 out of 24 metabolites measured) including ornithine, Alanine, Proline, Tryptophane,
441 Phenylalanine, thiamine, Lysine, glutamine, glutamic acid (Figure 5B). Similarly,
442 SynComs 20, 27, and 40 showed high consumption of amino acids such as glycine,
443 alanine, and glutamic acid.
444
445 **Discussion**
446 In this study, we assembled synthetic communities (SynComs) from 10 prevalent
447 human nasal bacterial species (*Anaerococcus octavius, Corynebacterium accolens,*
448 *Corynebacterium propinquum, Corynebacterium pseudodiphtheriticum,*
449 *Corynebacterium tuberculostearicum, Cutibacterium acnes, Cutibacterium avidum,*
450 *Dolosigranulum pigrum, Staphylococcus epidermidis, and Staphylococcus*
451 *lugdunensis*). Our unbiased assembly strategy allowed us to test whether nasal
452 community state types arise as intrinsic ecological attractors. Additionally, we
453 evaluated how community composition and strain-level variation influence stability of
454 these SynComs over time (four time points across 12 days) and resistance to invasion
455 of *S. aureus* at the final time point.
456

457 Multistability has been documented across microbial communities, where interaction-
458 driven population dynamics and feedback loops generate alternative taxonomic states
459 [45, 46]. In the case of the nasal microbiome, community state types (CSTs) have been
460 described based on a species level [26]. However, comparison with the HMP dataset
461 suggests that CST boundaries are diffuse, indicating that additional sources of
462 variability shape nasal community composition than previously thought. In the case of
463 our SynComs experiment, three distinct community clusters emerged despite random
464 assembly, suggesting that deterministic ecological processes play an important role in
465 community dynamics. These clusters can be interpreted as three alternative stable
466 states, each representing similar community compositions towards which the different
467 combinations of species and strains tend to converge.
468
469 The clusters differed in species richness, evenness, and dominant taxa, and showed
470 markedly different levels of resistance to *S. aureus* colonization. Importantly, our panel
471 of cultivated SynComs reproduced several characteristics observed in the HMP
472 dataset and the previously described CSTs of the nasal microbiome (Figure S1). In
473 particular, we observed the frequent coexistence of *Corynebacterium* species, the
474 persistence of *D. pigrum* (although represented by a single strain), and the overall
475 unevenness typical of nasal communities. Together, these findings demonstrate that
476 the ability of the nasal microbiome to resist *S. aureus* colonization can be recapitulated
477 and studied under controlled *in vitro* conditions, making our SynComs a platform for
478 systematic and mechanistic analyses of the nasal microbiota dynamics.
479
480 The observation that SynComs dominated by *C. propinquum* showed stronger
481 colonization resistance against *S. aureus* is consistent with previous studies showing
482 that nasal communities dominated by *Corynebacterium* spp. (including *C. propinquum*)

483 are often associated with reduced *S. aureus* carriage, potentially through production of
484 siderophores and other competitive factors that limit *S. aureus* growth [8, 11, 13, 47].
485 Analysis of the HMP data supports this hypothesis and shows that species identities
486 are not the only predictive factor of colonization resistance. Our SynCom experiments
487 show three examples of strain-level effects: (1) SynComs with the same species
488 composition, but with different strains, resulted in different final compositions (for
489 example SC1 of Cluster 1, SC29 of Cluster 2, SC5 of Cluster 3); (2) *C. propinquum*
490 strains 16 and 265 consistently dominated SynComs, whereas strain 70 did not and
491 (3) *D. pigrum* strain 21 was the only strain of that species which could persist
492 throughout the entire experiment. Together with the high variability of *C. propinquum*
493 abundance across the HMP cohort, ranging from very low relative abundance to >70%
494 in some individuals, these findings suggest that strain-level characteristics are
495 important for nasal microbiome composition and function. Our data shows that
496 differences between strains (presumably their metabolic capacities) influences their
497 ability to dominate and persist. Thus, future studies could map this to specific metabolic
498 capacities of the different strains, e.g. biosynthetic pathways for amino acids or
499 siderophores. For example, it has been shown that mutations in biosynthetic genes
500 can lead to strain-specific auxotrophies [48]. The same is true for other species, such
501 as *S. lugdunensis* or *D. pigrum*, for which only some strains have shown inhibitory
502 capacities against *S. aureus* [9, 49, 50].
503
504 *D. pigrum* is another key species in the nasal environment, ranking as the eighth most
505 prevalent species in the HMP cohort data. It has been noted as promoting colonization
506 resistance through modulation of the local microenvironment and production of
507 antimicrobial factors [9, 50]. Moreover, *D. pigrum* has been reported to engage in
508 positive interactions with *Corynebacterium* species, particularly *C.*

509 *pseudodiphtheriticum* [9, 51]. Our SynCom data support these observations, as *D.*
510 *pigrum* was only present in SynComs when *C. pseudodiphtheriticum* and *C. accolens*
511 were also present (SynComs 19, 25, 27, 44 and 50; Figure 2). While the mechanistic
512 basis of these associations remains unclear, understanding such cooperative
513 interactions is important given their potential synergistic effects against pathogens
514 such as *S. aureus*.
515
516 In addition to Corynebacteria and *D. pigrum*, staphylococcal species, such as *S.*
517 *epidermidis* and *S. lugdunensis*, are known to inhibit *S. aureus* through production of
518 antimicrobial peptides and direct interference [49, 52–54]. In our SynComs, rather than
519 observing isolated effects of individual species, we found evidence for synergistic
520 interactions between these two staphylococci due to their consistent coexistence in the
521 SynComs (SynComs 5, 7, 21, 26, 27, 34, 36, 40, 50; Figure 2). Such potential
522 cooperative effects have been described in previous research in the context of the
523 nasal environment and the respiratory tract, for example, synergism between *D.*
524 *pigrum* and *C. pseudodiphtheriticum* [51], or siderophore sharing between
525 staphylococcal species [47]. These results suggest that colonization resistance in the
526 nasal cavity is likely an emergent property of multiple interacting species and strains,
527 and probably driven by both competition and cooperation.
528
529 Our study also shows that it is possible to quantify both primary and secondary
530 metabolites in nasal SynComs. These metabolome analyses provide additional
531 insights into potential mechanisms underlying colonization resistance. SynComs in
532 Cluster 1, dominated by *C. propinquum*, were enriched in the siderophore
533 deferoxamine E. Genome analysis further revealed a high-confidence NI-siderophore
534 biosynthetic gene cluster with strong similarity to the dehydroxynocardamine pathway,

535 consistent with the production of deferoxamine E. This siderophore may contribute to
536 iron depletion and thereby limit *S. aureus* growth. Previous studies have demonstrated
537 that iron sequestration by siderophores is an important competitive mechanism of
538 corynebacteria in nasal ecosystems [13, 47, 55, 56]. Moreover, we observed changes
539 in the abundance of nutrients, such as amino acids and riboflavin, that were highly
540 specific for some SynComs, suggesting that nutrient competition may further contribute
541 to colonization resistance. We identified alanine, glutamic acid, tyrosine, glycine and
542 riboflavin as important nutritional metabolites for *S. aureus* USA300. These results are
543 consistent with studies reporting that *S. aureus* growth is constrained by amino acid
544 availability in nutrient-limited environments and by the fact that the nasal cavity is
545 naturally poor in amino acids [10, 25, 55].
546
547 Our pairwise coculture experiments with *C. propinquum* and *S. aureus* further support
548 the hypothesis that nutritional conditions influence the competitive dynamics between
549 the two bacteria. Under the poor nutritional conditions of SNM3, *C. propinquum* strains
550 16 and 265 successfully outcompeted *S. aureus*. In contrast, the nutrient-rich medium
551 BHI allowed *S. aureus* to overgrow all *C. propinquum* strains. These contrasting
552 outcomes suggest that differences in nutrient availability shape the relative fitness of
553 the two species.
554
555 One possible explanation is that *C. propinquum* is adapted to the nutritionally limited
556 environment of the nasal cavity, potentially favoring efficient resource utilization, while
557 *S. aureus* may be better suited to rapid growth under nutrient-rich conditions. Although
558 this hypothesis remains to be directly tested, it is consistent with expectations from the
559 r/K selection theory [57] where the slow-growing K-strategists (in this case *C.*
560 *propinquum* strains) specialize in surviving under poor-nutrient conditions and r-

561 strategists (*S. aureus* in this scenario) maximize their growth rate in nutrient rich
562 scenarios. r/K strategies have been observed in other microbial systems, like soil
563 communities, as important for community structure and functioning [58, 59]. Further,
564 this context-dependent competitive outcome is a widely reported phenomenon,
565 demonstrating that competition for specific limiting nutrients, such as essential metal
566 cofactors or amino acids, mediates colonization resistance. An example of this was
567 reported as a colonization resistance mechanism in the gut microbiome against
568 *Salmonella* [60]. Additionally, our observation that strains 16 and 265 grow better than
569 strain 70 both in single and in SynCom cultures suggests that intrinsic strain-level
570 differences are important factors of competitive success. Together, these results
571 indicate that both environmental constraints (e.g. nutrient availability) and strain
572 specific factors (e.g. biosynthetic or catabolic capacities) determine the ability of *C.*
573 *propinquum* to inhibit *S. aureus*, providing an explanation for the strain-dependent
574 protection observed in our SynCom experiments.
575
576 The reproducibility of our SynCom approach shows that they are a tractable model
577 system for controlled and systematic investigations of nasal microbiome ecology. Until
578 now, most studies examining the effects of specific taxa on *S. aureus* have used
579 isolated pairs of strains, and here we expand this to a broader community context. Our
580 work highlights how strain-level diversity, species co-occurrence, and metabolic
581 interactions collectively shape colonization outcomes.
582
583 *Limitations and Future Directions*
584 Our study has several limitations. First, our SynComs were assembled from a limited
585 culture collection of 10 species, which, while representing some of the most prevalent
586 members of the nasal microbiome, does not capture its full diversity. Fastidious or

587 currently unculturable taxa, not present in the LaCa collection, were necessarily
588 excluded. Our experimental setting did not reproduce the anaerobic
589 microenvironments present in the nasal cavity, and as a result two (*A. octavius* and *C.*
590 *acnes*) of the three anaerobic species failed to grow in any SynCom. These anaerobes
591 have been implicated in community structure and may influence *S. aureus* dynamics
592 [61]. Furthermore, only one strain of *S. aureus* was used in our invasion test. Use of
593 other strains of *S. aureus* could help elucidate the strain-dependent mechanisms of
594 invasion success for this species.
595
596 Second, our experiments were performed entirely *in vitro*, which does not fully
597 recapitulate the nasal mucosal environment, host immune responses, or spatial
598 structure that may modulate microbial interactions and metabolite diffusion, as has
599 been shown for other microbial ecosystems. Future studies should expand SynCom
600 designs to include additional, fastidious species and incorporate host-derived factors
601 such as epithelial cells, immune components, or human organoids, as has been done
602 in porcine nasal microbiome models [62]. Incorporating physical structure into
603 experimental setups is necessary, as it could help establish microaerophilic or
604 anaerobic niches that support the growth of strict anaerobes and more closely mimic
605 in vivo spatial organization which influences ecological interactions and dynamics [63,
606 64]. Finally, while our metabolomics analysis identified metabolites associated with
607 specific community clusters, a substantial proportion of detected features remain
608 unannotated, which limits mechanistic interpretation. Future work combining targeted
609 metabolomics and genetic perturbations will be essential to confirm the specific roles
610 of siderophores and amino acid competition in mediating *S. aureus* exclusion.
611

612 In summary, we demonstrate that nasal SynComs reproduce key compositional
613 and functional features of the human nasal microbiome, including the emergence of
614 distinct community states with variable resistance to *S. aureus* colonization. Our
615 findings highlight the importance of both species and strain identity in shaping
616 community assembly and function and suggest that nutritional competition particularly
617 for iron and amino acids is a critical mechanism driving colonization resistance in a
618 community context. These results provide a basis for the rational design of
619 microbiome-based interventions aimed at reducing *S. aureus* carriage and preventing
620 infection. By integrating SynCom approaches with host-microbe models and *in vivo*
621 validation, future research can further elucidate the ecological principles governing
622 nasal microbiome stability and pathogen exclusion.
623

624 **Acknowledgements**

625 We thank Dr. Anna Walke from Agilent Technologies (Germany, Waldbronn) for her
626 guidance on the targeted LC-MS/MS Agilent method. This work was funded by the
627 Deutsche Forschungsgemeinschaft (DFG, German Research Foundation) under
628 Germanýs Excellence Strategy – EXC 2124 – 390838134 (M.N.D, S.H., D.P., L.C.,
629 L.T.A., H.L., S.He.).
630

631 **Data availability**

632 Data and code for analyses are available on GitHub at: https://github.com/marcelo-
633 nd/nasalSynComs.
634
635

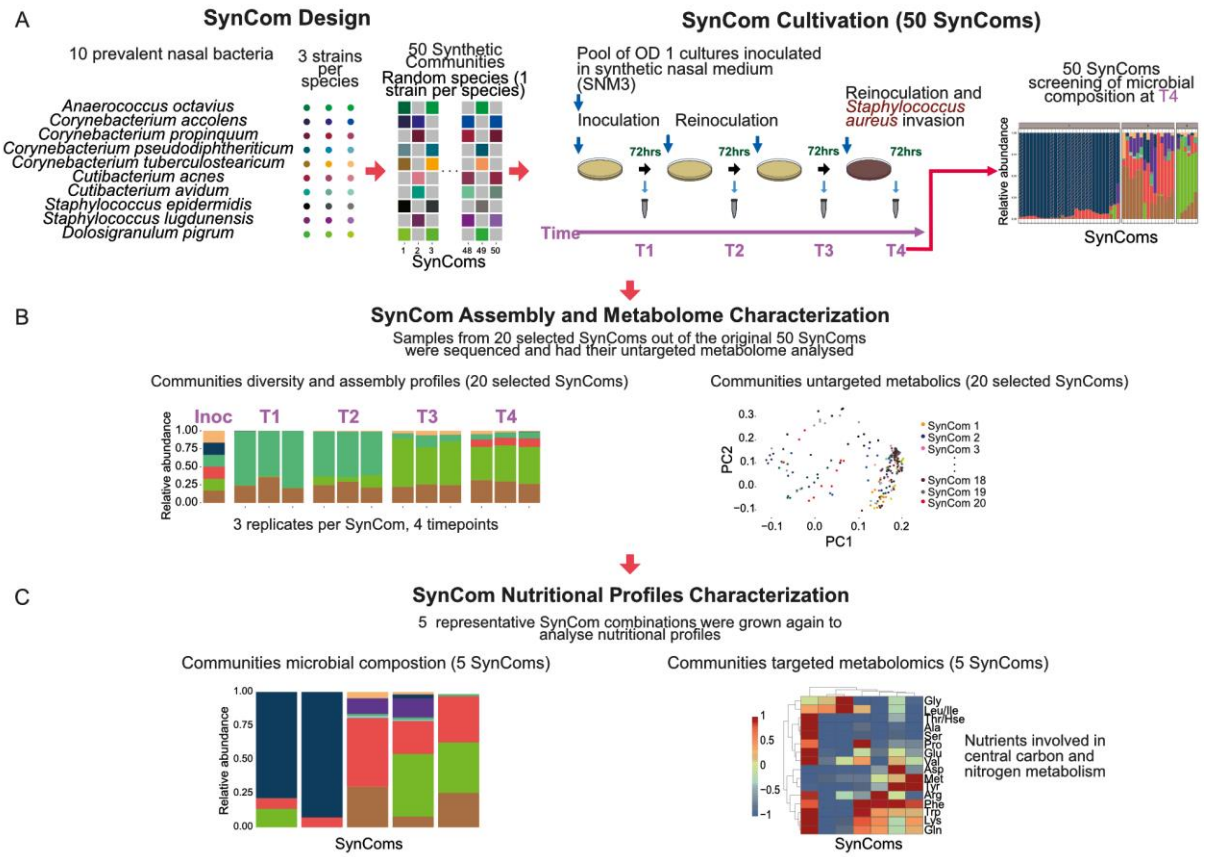

Figure 1. SynCom design and experimental workflow. (A) Ten of the most prevalent nasal bacterial species, each represented by three strains, were selected based on analyses of Human Microbiome Project data and the strain availability in the LaCa collection of nasal isolates [25]. SynComs were assembled by randomly selecting both the number (from 5 to 10) and identity of species per community, followed by the random selection of one strain per species. Communities were cultivated on Synthetic Nasal Medium agar plates (SNM3;[10]). SynComs were grown for 72 h, after which biomass was collected for reinoculation, DNA extraction and sequencing, and metabolomics analyses. Three sequential reinoculations on fresh SNM3 plates were performed. In the final reinoculation, *S. aureus* was introduced to assess colonization resistance. SynCom composition was determined using Nanopore sequencing. (B) Twenty selected communities were further characterized across all time points and replicates using sequencing and untargeted metabolomics to investigate assembly dynamics and metabolome composition. (C) Finally, five representative SynCom combinations were grown again from scratch to examine nutrient production and consumption profiles using targeted metabolomics.

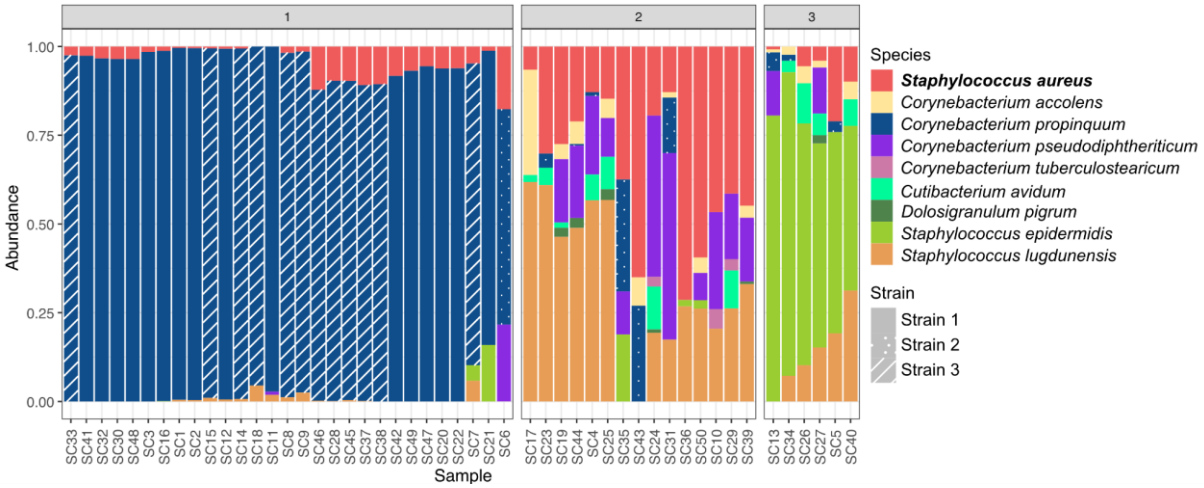

Figure 2. Screening of SynCom composition and assembly into stable clusters. Relative abundance barplots show the microbial composition of the 50 assembled SynComs at the final study time point (72 h after *S. aureus* inoculation). To screen the ecological behavior across the broad compositional landscape of the SynComs, one replicate per SynCom was characterized. Samples are ordered along the x-axis according to Euclidean-distance clustering of relative abundance data. The optimal number of clusters (k=3) was determined using the silhouette method, identifying distinct compositional attractors. Strain-level variation is specifically highlighted for *C. propinquum* and *D. pigrum* using distinct barplot patterns.

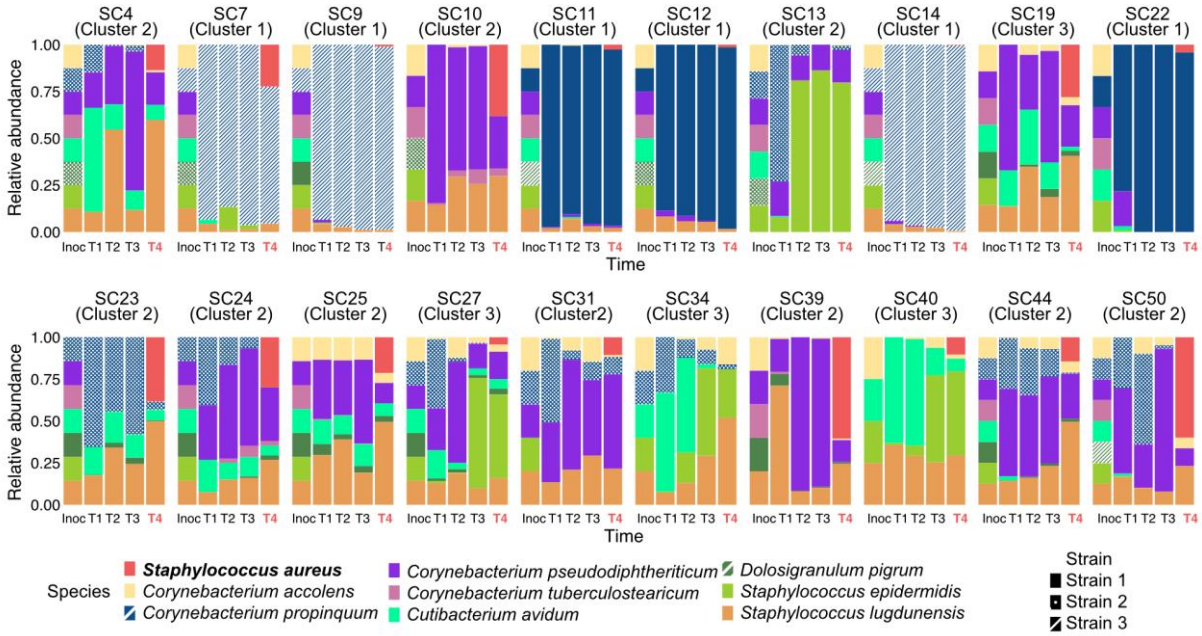

Figure 3. Temporal dynamics of bacterial community composition in 20 selected SynComs. Samples of 20 SynComs were selected out of the 50 in the main experiment and community composition was characterized by sequencing at four time points across the experiment. Samples from these 20 SynComs were also analyzed using untargeted metabolomics. Each panel represents one SynCom and shows relative abundance barplots for one replicate per SynCom over time. Barplot patterns indicate which of the three strains was inoculated for *C. propinquum* and *D. pigrum*. Strain level information of other species is not shown.

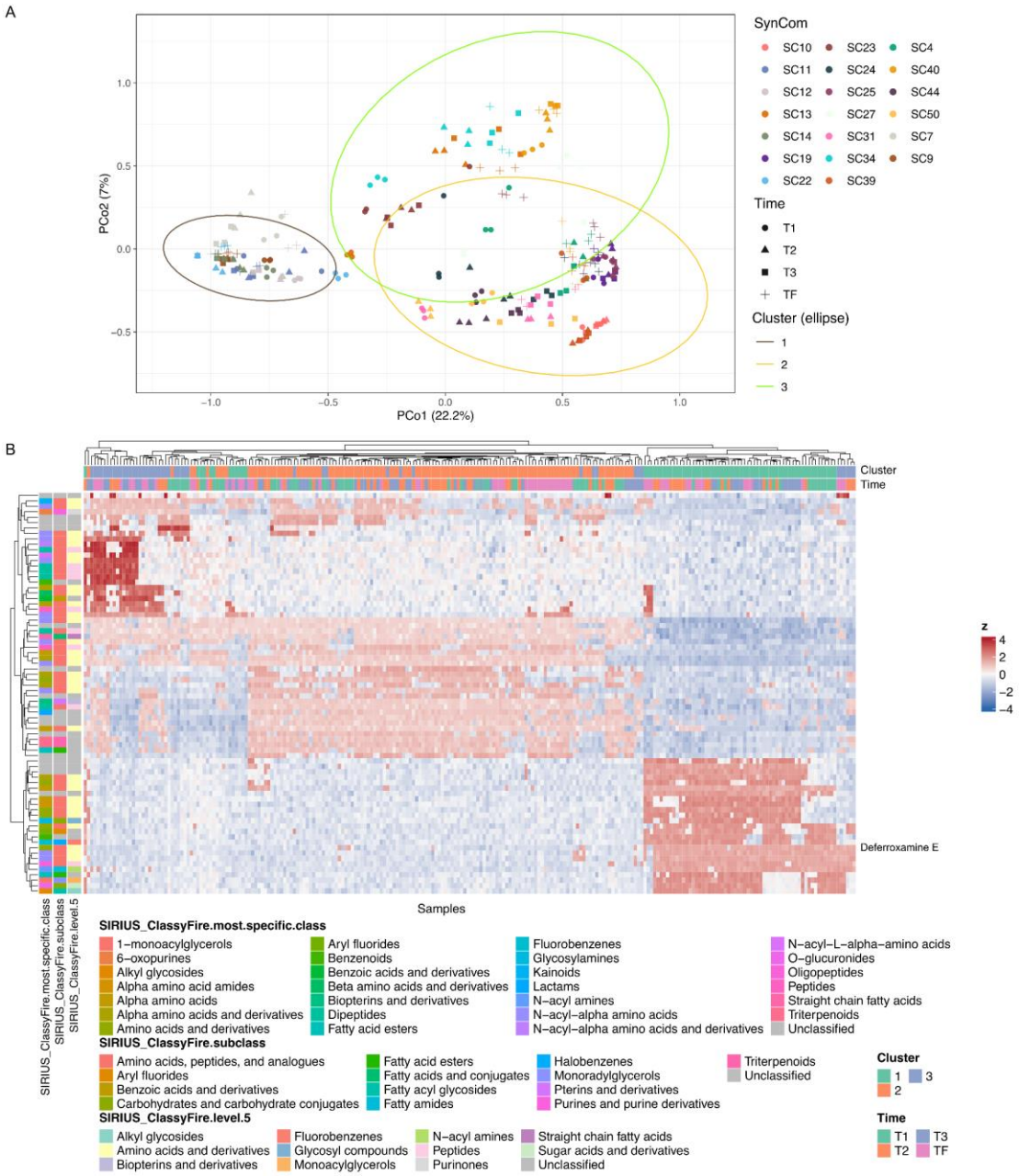

Figure 4. Compositional similarity and metabolic profiles of the 20 selected SynComs. For 20 of the original 50 SynComs, community composition was characterized and untargeted metabolomics analyses were performed at four time points across the experiment and 3 replicates (240 samples). (A) Principal coordinates analysis (PCoA) of bacterial community composition for samples from the 20 selected SynComs. The ordination is based on pairwise dissimilarities in relative abundances. Each point represents one sample and replicate (3 per SynCom in each timepoint); colors indicate SynCom identity, point shapes indicate the time point from which the samples were taken and 95% confidence ellipses denote the SynCom composition clusters. (B) Heatmap of the top 30 metabolite features associated with SynCom clusters, identified using a limma-based linear modeling approach using the limma package for R [40]. The column annotation above the heatmap indicates the cluster assignment of each sample and the time point from which they were taken. Row annotations on the left indicate predicted metabolite classes as assigned by the SIRIUS CANOPUS algorithm. Metabolite signals are displayed as standardized values (row-wise z-scores of log-transformed intensities).

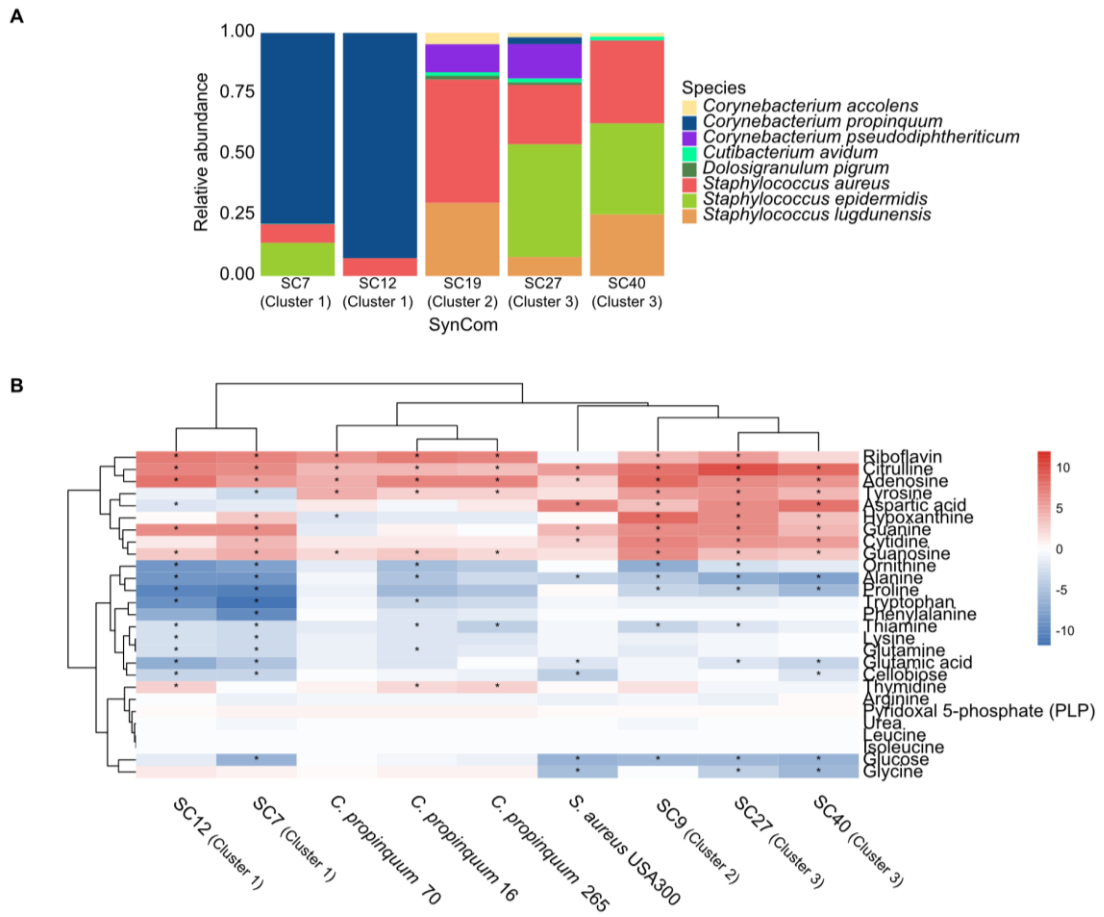

Figure 5. Bacterial composition and targeted metabolite profiles of five selected SynComs, *S. aureus* USA300 and the three strains of *C. propinquum* used in SynCom experiments. Five SynComs selected from the main screen were grown again in 12-well plates to quantify metabolite production and consumption by targeted metabolomics. In parallel, monocultures of *S. aureus* USA300 (used to test colonization resistance) and the three *C. propinquum* strains were cultivated in the same format and analyzed alongside the SynComs. (A) Relative abundance barplots showing the bacterial composition of the five selected SynComs. (B) Heatmap of $\log_2$ fold-change in mean metabolite abundance relative to the medium-only control (SNM3 without inoculation). For each metabolite and condition, $\log_2$ fold-changes were computed from mean intensities across replicates. Asterisks indicate metabolites that differ significantly from the control based on Welch's t-tests on $\log_2$-transformed replicate intensities with Benjamini–Hochberg correction (FDR < 0.05) and an absolute $\log_2$ fold-change ≥ 2 (≥ 4-fold change).

References

1. Caballero-Flores G, Pickard JM, Núñez G. Microbiota-mediated colonization resistance: mechanisms and regulation. *Nat Rev Microbiol* 2023;**21**:347–360. https://doi.org/10.1038/s41579-022-00833-7

2. Sarkar S et al. A Review on the Nasal Microbiome and Various Disease Conditions for Newer Approaches to Treatments. *Indian J Otolaryngol Head Neck Surg* 2023;**75**:755–763. https://doi.org/10.1007/s12070-022-03205-y

3. Sakr A et al. Staphylococcus aureus Nasal Colonization: An Update on Mechanisms, Epidemiology, Risk Factors, and Subsequent Infections. *Front Microbiol* 2018;**9**:2419. https://doi.org/10.3389/fmicb.2018.02419

4. Eiff CV, Peters G. Nasal Carriage as a Source of Staphylococcus aureus Bacteremia. 2001.

5. Duhaniuc A et al. Multidrug-Resistant Bacteria in Immunocompromised Patients. *Pharmaceuticals* 2024;**17**:1151. https://doi.org/10.3390/ph17091151

6. Chand U, Priyambada P, Kushawaha PK. Staphylococcus aureus vaccine strategy: Promise and challenges. *Microbiol Res* 2023;**271**:127362. https://doi.org/10.1016/j.micres.2023.127362

7. Van Dalen R et al. Secretory IgA impacts the microbiota density in the human nose. *Microbiome* 2023;**11**:233. https://doi.org/10.1186/s40168-023-01675-y

8. Laux C, Peschel A, Krismer B. *Staphylococcus aureus* Colonization of the Human Nose and Interaction with Other Microbiome Members. *Microbiol Spectr* 2019;**7**:7.2.34. https://doi.org/10.1128/microbiolspec.GPP3-0029-2018

9. Brugger SD et al. Dolosigranulum pigrum Cooperation and Competition in Human Nasal Microbiota. *mSphere* 2020;**5**:e00852-20. https://doi.org/10.1128/mSphere.00852-20

10. Krismer B et al. Nutrient Limitation Governs Staphylococcus aureus Metabolism and Niche Adaptation in the Human Nose. *PLoS Pathog* 2014;**10**:e1003862. https://doi.org/10.1371/journal.ppat.1003862

11. Tamkin E et al. Airway *Corynebacterium* interfere with *Streptococcus pneumoniae* and *Staphylococcus aureus* infection and express secreted factors selectively targeting each pathogen. *Infect Immun* 2025;**93**:e00445-24. https://doi.org/10.1128/iai.00445-24

12. Krismer B et al. The commensal lifestyle of Staphylococcus aureus and its interactions with the nasal microbiota. *Nat Rev Microbiol* 2017;**15**:675–687. https://doi.org/10.1038/nrmicro.2017.104

13. Zhao Y et al. Nasal commensals reduce *Staphylococcus aureus* proliferation by restricting siderophore availability. *ISME J* 2024;**18**:wrae123. https://doi.org/10.1093/ismejo/wrae123

14. Proctor DM, Relman DA. The Landscape Ecology and Microbiota of the Human Nose, Mouth, and Throat. *Cell Host Microbe* 2017;**21**:421–432. https://doi.org/10.1016/j.chom.2017.03.011

15. Hardy BL, Merrell DS. Friend or Foe: Interbacterial Competition in the Nasal Cavity. *J Bacteriol* 2021;**203**. https://doi.org/10.1128/JB.00480-20

16. Faith JJ et al. The Long-Term Stability of the Human Gut Microbiota. *Science* 2013;**341**:1237439. https://doi.org/10.1126/science.1237439

17. Venturelli OS et al. Deciphering microbial interactions in synthetic human gut microbiome communities. *Mol Syst Biol* 2018;**14**:e8157. https://doi.org/10.15252/msb.20178157

18. Bai Y et al. Functional overlap of the Arabidopsis leaf and root microbiota. *Nature* 2015;**528**:364–369. https://doi.org/10.1038/nature16192

19. Niu B et al. Simplified and representative bacterial community of maize roots. *Proc Natl Acad Sci* 2017;**114**. https://doi.org/10.1073/pnas.1616148114

20. Goodman AL et al. Extensive personal human gut microbiota culture collections characterized and manipulated in gnotobiotic mice. *Proc Natl Acad Sci* 2011;**108**:6252–6257. https://doi.org/10.1073/pnas.1102938108

21. Pacheco AR, Osborne ML, Segrè D. Non-additive microbial community responses to environmental complexity. *Nat Commun* 2021;**12**:2365. https://doi.org/10.1038/s41467-021-22426-3

22. Weiss AS et al. In vitro interaction network of a synthetic gut bacterial community. *ISME J* 2022;**16**:1095–1109. https://doi.org/10.1038/s41396-021-01153-z

23. Buffie CG et al. Precision microbiome reconstitution restores bile acid mediated resistance to Clostridium difficile. *Nature* 2015;**517**:205–208. https://doi.org/10.1038/nature13828

24. Bonillo-Lopez L et al. *In vitro* metabolic interaction network of a rationally designed nasal microbiota community. 2024. Systems Biology, 2024.

25. Camus L et al. Tyrosine availability shapes Staphylococcus aureus nasal colonization and interactions with commensal communities. *bioRxiv* 2025;2025.05.06.651429. https://doi.org/10.1101/2025.05.06.651429

26. Liu CM et al. *Staphylococcus aureus* and the ecology of the nasal microbiome. *Sci Adv* 2015;**1**:e1400216. https://doi.org/10.1126/sciadv.1400216

27. Turnbaugh PJ et al. The Human Microbiome Project. *Nature* 2007;**449**:804–810. https://doi.org/10.1038/nature06244

28. Estaki M et al. QIIME 2 Enables Comprehensive End-to-End Analysis of Diverse Microbiome Data and Comparative Studies with Publicly Available Data. *Curr Protoc Bioinforma* 2020;**70**:e100. https://doi.org/10.1002/cpbi.100

29. Callahan BJ et al. DADA2: High-resolution sample inference from Illumina amplicon data. *Nat Methods* 2016;**13**:581–583. https://doi.org/10.1038/nmeth.3869

30. Camacho C et al. BLAST+: architecture and applications. *BMC Bioinformatics* 2009;**10**:421. https://doi.org/10.1186/1471-2105-10-421

31. Goldfarb T et al. NCBI RefSeq: reference sequence standards through 25 years of curation and annotation. *Nucleic Acids Res* 2025;**53**:D243–D257. https://doi.org/10.1093/nar/gkae1038

32. Aguayo-Reyes A et al. Emergence of ST8-USA300 and ST8-USA300-Latin American variant: a changing landscape of community-associated methicillin-resistant *Staphylococcus aureus* in Chile. *Microbiol Spectr* 2025;**13**:e01031-25. https://doi.org/10.1128/spectrum.01031-25

33. Seol D et al. Microbial Identification Using rRNA Operon Region: Database and Tool for Metataxonomics with Long-Read Sequence. *Microbiol Spectr* 2022;**10**:e02017-21. https://doi.org/10.1128/spectrum.02017-21

34. Curry KD et al. Emu: species-level microbial community profiling of full-length 16S rRNA Oxford Nanopore sequencing data. *Nat Methods* 2022;**19**:845–853. https://doi.org/10.1038/s41592-022-01520-4

35. Rice P, Longden I, Bleasby A. EMBOSS: The European Molecular Biology Open Software Suite. *Trends Genet* 2000;**16**:276–277. https://doi.org/10.1016/S0168-9525(00)02024-2

36. Schmid R et al. Integrative analysis of multimodal mass spectrometry data in MZmine 3. *Nat Biotechnol* 2023;**41**:447–449. https://doi.org/10.1038/s41587-023-01690-2

37. Nothias L-F et al. Feature-based molecular networking in the GNPS analysis environment. *Nat Methods* 2020;**17**:905–908. https://doi.org/10.1038/s41592-020-0933-6

38. Dührkop K et al. Systematic classification of unknown metabolites using high-resolution fragmentation mass spectra. *Nat Biotechnol* 2021;**39**:462–471. https://doi.org/10.1038/s41587-020-0740-8

39. Dührkop K et al. SIRIUS 4: a rapid tool for turning tandem mass spectra into metabolite structure information. *Nat Methods* 2019;**16**:299–302. https://doi.org/10.1038/s41592-019-0344-8

40. Yannell, Karen, Hsiao, Jordy, Cuthbertson, Dan. Mastering HILIC-Z Separation for Polar Analytes. 2023. USA: Agilent Technologies, Inc., 2023.

41. Maechler M et al. cluster: Cluster analysis basics and extensions (R package version 2.1.1). 2021. 2021.

42. Rousseeuw PJ. Silhouettes: A graphical aid to the interpretation and validation of cluster analysis. *J Comput Appl Math* 1987;**20**:53–65. https://doi.org/10.1016/0377-0427(87)90125-7

43. Ritchie ME et al. limma powers differential expression analyses for RNA-sequencing and microarray studies. *Nucleic Acids Res* 2015;**43**:e47–e47. https://doi.org/10.1093/nar/gkv007

44. Wickham H. ggplot2 Elegant Graphics for Data Analysis, 2nd edn. Springer Cham, 2016.

45. Gonze D et al. Multi-stability and the origin of microbial community types. *ISME J* 2017;**11**:2159–2166. https://doi.org/10.1038/ismej.2017.60

46. Estrela S et al. Functional attractors in microbial community assembly. *Cell Syst* 2022;**13**:29-42.e7. https://doi.org/10.1016/j.cels.2021.09.011

836 47. Stubbendieck RM et al. Competition among Nasal Bacteria Suggests a Role
837 for Siderophore-Mediated Interactions in Shaping the Human Nasal Microbiota. *Appl*
838 *Environ Microbiol* 2019;**85**:e02406-18. https://doi.org/10.1128/AEM.02406-18

839 48. Lubrano P et al. Metabolic mutations reduce antibiotic susceptibility of E.
840 coli by pathway-specific bottlenecks. *Mol Syst Biol* 2025;**21**:274–293.
841 https://doi.org/10.1038/s44320-024-00084-z

842 49. Heilbronner S. Staphylococcus lugdunensis. *Trends Microbiol*
843 2021;**29**:1143–1145. https://doi.org/10.1016/j.tim.2021.07.008

844 50. Cole AL et al. Nasal microbiome inhabitants with anti- *Staphylococcus*
845 *aureus* activity. *Microbiol Spectr* 2025;e01024-25.
846 https://doi.org/10.1128/spectrum.01024-25

847 51. Cisneros M et al. Synergistic inhibition of pneumococcal growth by
848 *Dolosigranulum pigrum* and *Corynebacterium pseudodiphtheriticum:* insights into
849 nasopharyngeal microbial interactions. *Microbiol Spectr* 2025;**13**:e00138-25.
850 https://doi.org/10.1128/spectrum.00138-25

851 52. Liu C-C et al. Defects in energy metabolism increase the susceptibility of
852 *Staphylococcus aureus* and its small colony variants (SCVs) to *Staphylococcus*
853 *lugdunensis* and lugdunin. *Microbiol Spectr* 2025;e01006-25.
854 https://doi.org/10.1128/spectrum.01006-25

855 53. Bessesen MT. Interventions targeting the nasal microbiome to eradicate
856 methicilin-resistant Staphylococcus aureus. *Clin Microbiol Infect* 2025;**31**:190–193.
857 https://doi.org/10.1016/j.cmi.2024.10.022

858 54. Liu Q et al. Staphylococcus epidermidis Contributes to Healthy Maturation
859 of the Nasal Microbiome by Stimulating Antimicrobial Peptide Production. *Cell Host*
860 *Microbe* 2020;**27**:68-78.e5. https://doi.org/10.1016/j.chom.2019.11.003

861 55. Adolf LA, Heilbronner S. Nutritional Interactions between Bacterial Species
862 Colonising the Human Nasal Cavity: Current Knowledge and Future Prospects.
863 *Metabolites* 2022;**12**:489. https://doi.org/10.3390/metabo12060489

864 56. Rosenstein R et al. The Staphylococcus aureus-antagonizing human nasal
865 commensal Staphylococcus lugdunensis depends on siderophore piracy.
866 *Microbiome* 2024;**12**:213. https://doi.org/10.1186/s40168-024-01913-x

867 57. Bongers T. The Maturity Index, the evolution of nematode life history traits,
868 adaptive radiation and cp-scaling. *Plant Soil* 1999;**212**:13–22.

869 58. Wang Y et al. Recovery of bacterial network complexity and stability after
870 simulated extreme rainfall is mediated by K−/r-strategy dominance. *Appl Soil Ecol*
871 2024;**203**:105657. https://doi.org/10.1016/j.apsoil.2024.105657

872 59. Zheng W et al. The response patterns of r- and K-strategist bacteria to long-
873 term organic and inorganic fertilization regimes within the microbial food web are
874 closely linked to rice production. *Sci Total Environ* 2024;**942**:173681.
875 https://doi.org/10.1016/j.scitotenv.2024.173681

876 60. Bushman SD, Skaar EP. The exploitation of nutrient metals by bacteria for
877 survival and infection in the gut. *PLOS Pathog* 2025;**21**:e1013580.
878 https://doi.org/10.1371/journal.ppat.1013580

879 61. Lucas SK et al. Anaerobic Microbiota Derived from the Upper Airways
880 Impact Staphylococcus aureus Physiology. *Infect Immun* 2021;**89**:e00153-21.
881 https://doi.org/10.1128/IAI.00153-21

882 62. Bonillo-Lopez L et al. Porcine nasal organoids to model interactions
883 between the swine nasal microbiota and the host. *Microbiome* 2025;**13**:131.
884 https://doi.org/10.1186/s40168-025-02088-9

885 63. Vallespir Lowery N, Ursell T. Structured environments fundamentally alter
886 dynamics and stability of ecological communities. *Proc Natl Acad Sci* 2019;**116**:379–
887 388. https://doi.org/10.1073/pnas.1811887116

888 64. Junkins EN et al. Environmental structure impacts microbial composition
889 and secondary metabolism. *ISME Commun* 2022;**2**:15.
890 https://doi.org/10.1038/s43705-022-00097-5